THE JOURNAL OF PHYSICAL CHEMISTRY Letters

Letter

pubs.acs.org/JPCL

Pressure-Induced Polymorphic, Optical, and Electronic Transitions of Formamidinium Lead Iodide Perovskite

Pan Wang,[†] Jiwen Guan,[‡] Draven T. K. Galeschuk,[§] Yansun Yao,[§,¶] Cindy F. He,[†] Shan Jiang,[†] Sijia Zhang,[#] Ying Liu,[#] Meiling Jin,[#] Changqing Jin,[#] and Yang Song*[,†,‡,∥]

[†]Department of Chemistry, The University of Western Ontario, London, Ontario N6A 5B7, Canada

[‡]Department of Physics and Astronomy, The University of Western Ontario, London, Ontario N6A 3K7, Canada

[§]Department of Physics and Engineering Physics, University of Saskatchewan, Saskatoon, Saskatchewan S7N 5E2, Canada

[¶]Canadian Light Source Inc., Saskatoon, Saskatchewan S7N 2V3, Canada

[#]Institute of Physics, Chinese Academy of Sciences, Beijing 100190, China

[∥]Soochow University−Western University Centre for Synchrotron Radiation Research, The University of Western Ontario, London, Ontario N6A 5B7, Canada

Supporting Information

ABSTRACT: Formamidinium lead iodide ($FAPbI_3$) perovskite as a superior solar cell material was investigated in two polymorphs at high pressures using in situ synchrotron X-ray diffraction, FTIR spectroscopy, photoluminescence (PL) spectroscopy, electrical conductivity (EC) measurements, and ab initio calculations. We identified two new structures (i.e., *Imm*2 and *Immm*) for α-$FAPbI_3$ but only a structural distortion (in *C*2/*c*) for δ-$FAPbI_3$ upon compression. A pressure-enhanced hydrogen bond plays a prominent role in structural modifications, as corroborated by FTIR spectroscopy. PL measurements and calculations consistently show the structure and pressure dependences of the band gap energies. Finally, EC measurements reveal drastically different transport properties of α- and δ-$FAPbI_3$ at low pressures but a common trend to metallic states at high pressures. All of these observations suggest strongly contrasting structural stabilities and pressure-tuned optoelectric properties of the two $FAPbI_3$ polymorphs.

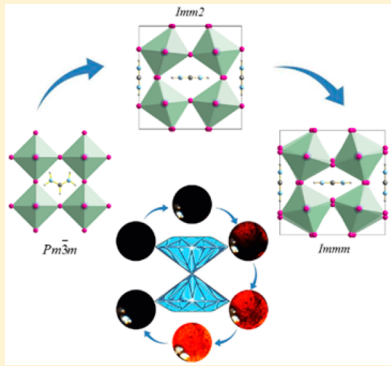

Recently, organometal halide perovskite-based solar cells have drawn enormous attention due to their superior properties and high power conversion efficiency (PCE).[1−3] Substantial efforts have been made over the past several years to improve the PCE (e.g., from 3.8 to 21.1%)[4] on methylammonium ($CH_3NH_3^+$ or MA) lead triiodide ($CH_3NH_3PbI_3$ or $MAPbI_3$) by tuning the band gap energy (1.5 to 2.3 eV) using different halide ions.[5,6] Compared to MA, the formamidinium cation ($NH_2CH{=}NH_2^+$ or FA) is slightly larger, and therefore, formamidinium lead triiodide ($FAPbI_3$) has a smaller band gap (1.45 eV), a broader absorption spectrum,[3,7−10] and ultimately a greater PCE in solar cells.[2] Currently, three polymorphs of $FAPbI_3$ are known at ambient conditions (i.e., α-, β-, and δ-phases).[11] The α-phase has a trigonal perovskite structure (space group *P*3*m*1), which is an excellent solar cell material over a broad solar spectrum.[11,12] The δ-$FAPbI_3$ has non-perovskite structure ($P6_3mc$) and is not suitable for photovoltaic applications due to a larger band gap (~2.48 eV).[13] Compared to the well-studied $MAPbI_3$, understanding of α-$FAPbI_3$ and its phase stabilities is still limited, which poses a challenge in the fabrication.[9]

Application of external static pressure can effectively alter the crystal structures and produce new polymorphs with improved photovoltaic properties and performance. In particular, solar cell materials modified under high pressures may possess novel and tunable electronic, optical, magnetic, and mechanical properties.[8,10,14−27] For instance, all MA-based perovskites undergo pressure-induced structural transitions and property changes.[10,14,16−19,21−23,26] The FA-based perovskites, on the other hand, have different behaviors at high pressures in that $FAPbBr_3$ undergoes phase transitions[15] whereas $FAPbI_3$ remains stable.[28] Moreover, the influence of the FA moiety in the perovskite materials remains unclear due to limited studies. Here we report a high-pressure investigation of α- and δ-$FAPbI_3$ by in situ synchrotron X-ray diffraction (XRD), Fourier transform infrared (FTIR) spectroscopy, photoluminescence (PL) spectroscopy, electrical conductivity (EC) measurements, and density functional theory (DFT) calculations. Our results reveal pressure-induced new polymorphs of $FAPbI_3$ with contrasting structural stabilities and properties. The demonstrated structure−property correlation provides practical guidance in the design and engineering of new solar cell materials.

Received: March 20, 2017
Accepted: April 25, 2017
Published: April 25, 2017

DOI: 10.1021/acs.jpclett.7b00665
J. Phys. Chem. Lett. 2017, 8, 2119−2125

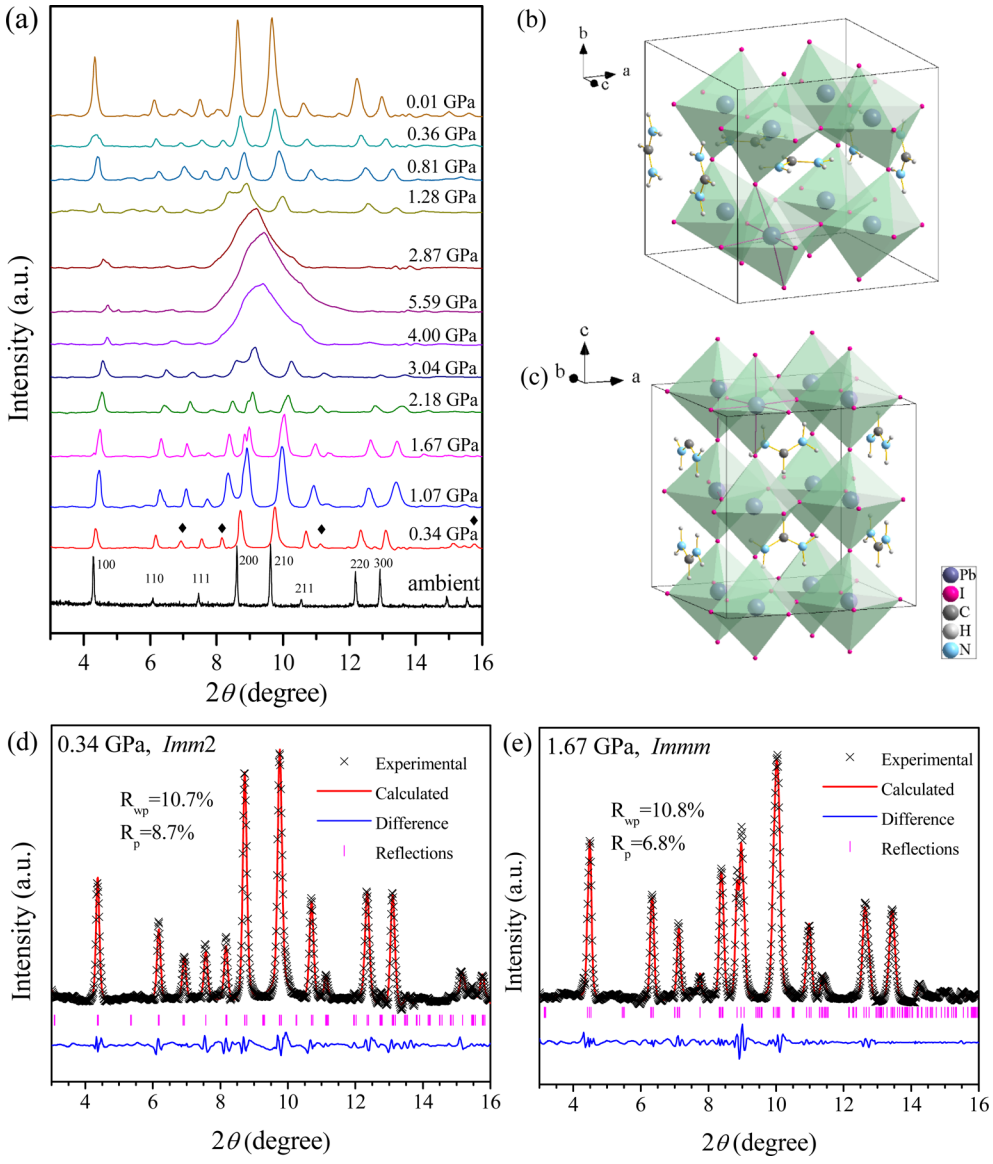

Figure 1. XRD patterns of α-$FAPbI_3$ upon compression and decompression (a), proposed crystal structures of high-pressure phase II (b) and phase III (c) based on MD simulations, and calculated XRD patterns in comparison with experimental results at 0.34 (d) and 1.67 GPa (e) using Rietveld refinement.

We synthesized both α- and δ-phase $FAPbI_3$ using the previously reported methods.[2,29] The XRD patterns of synthesized materials are in excellent agreement with the literature data indicating the high purity of as-made samples. Structural refinement suggests that the α-phase has a $Pm\bar{3}m$ structure, consistent with the recently reported cubic structure,[13] while the δ-phase has a $P6_3mc$ structure[2,11] (Figure S1). Figure 1a (Figure S3a) shows selected XRD patterns of α-$FAPbI_3$ (δ-$FAPbI_3$) at high pressure (see the SI for detailed XRD analysis for δ-$FAPbI_3$). At 0.34 GPa, the XRD pattern of α-$FAPbI_3$ exhibits new reflection peaks, indicating the formation of a new structure (designated as phase II). At 1.67 GPa, another new reflection appeared at 8.8° together with the asymmetrization of several other reflections, indicating the transition to another phase (phase III). The XRD pattern upon compression to 4 GPa displays a broad profile at 9.5°, indicating lattice amorphization, although a small portion of the sublattice remains crystalline, similar to other perovskite materials.[14−16,22] Upon decompression, remarkably, the recovered phase at near-ambient pressure exhibits a pattern similar to phase II instead of the ambient phase I (which can be refined using the phase II structure; see following and Table S1), indicating an irreversible transition. This observation is in direct contrast to the recently reported high-pressure behavior of $FAPbI_3$,[28] where a different starting structure was used, which showed no structural transitions at high pressure. The starting structure of α-$FAPbI_3$ is therefore highly sensitive to the detailed preparation procedures.

α-$FAPbI_3$ has been reported to gradually transform to the δ-phase at ambient conditions.[2,30] However, the diffraction patterns of phases II and III clearly do not match that of the δ-phase structure, indicating that both are new phases. We performed ab initio molecular dynamics (MD) simulations to search for possible structures for phases II and III. The simulation at ambient conditions reveals free rotations of FA molecules and an average cubic structure, consistent with experimental results. With increasing pressure, the interactions between FA and PbI_6 octahedra are enhanced, which leads to

DOI: 10.1021/acs.jpclett.7b00665
J. Phys. Chem. Lett. 2017, 8, 2119−2125

confined FA vibrations and unit cell distortions. The most probable structures discovered in the MD simulations for phases II and III are both orthorhombic with space groups *Imm*2 and *Immm*, respectively (Figure 1b,c). Using these structures, the calculated diffraction patterns excellently reproduced experimental data (Figure 1d,e), giving reduced cell parameters of a = 6.2475 Å, b = 6.2450 Å, and c = 6.2714 Å for phase II and a = 6.1132 Å, b = 6.0920 Å, and c = 6.1792 Å for phase III structures. Interestingly, the *Imm*2 structure for α-$FAPbI_3$ is similar to that of β-$FASnI_3$,[11] while the *Immm* structure is similar to a $MAPbI_3$ structure found favorable above 2.7 GPa.[16] In addition, the enthalpy calculation (Figure S2) indicates that *Imm*2 and *Immm* are indeed low-energy structures not only with increasing pressures but even at ambient pressure, consistent with the experimental observation that the recovered phase retains *Imm*2 structure. Upon compression, the first phase transition ($Pm\bar{3}m$ to *Imm*2) can be characterized by tilting between two adjacent PbI_6 octahedra as well as distortion of an individual PbI_6 octahedron leading to modified Pb−I−Pb angles (166.8, 144.0, and 177.8°). The subsequent *Imm*2-to-*Immm* transition features a further distortion of the unit cell, leading to considerable change of Pb−I−Pb angles to 143.0 and 154.5° but no tilting along the c-axis (i.e., the Pb−I−Pb angle remains 180°). The unit cell parameters as a function of pressure (Table S1 and Figure S5) suggest that the first transition is smooth and continuous but the second transition at 1.67 GPa has an unusual expansion of the c-axis and an anomaly of the unit cell volume at the phase boundary. This unusual behavior could be associated with tilting of the PbI_6 polyhedron as a result of anisotropic compressibility of the crystal axes (see below).

To explore the pressure effects on the FA moiety and cation−anion interactions, we performed in situ FTIR spectroscopy (Figures 2 and S6). In the mid-IR region, the optical absorption is exclusively attributed to vibrations from organic FA ($H_2N^+{=}CHNH_2$) (Table S2). Upon compression, the pressure dependence (Table S3) collectively exhibits discontinuities at 0.5 and 1.7 GPa for α-$FAPbI_3$, in agreement with the identified transition boundaries. The pressure-induced profile broadening above 4 GPa is also consistent with the structural amorphization suggested by XRD measurements. Most of observed IR modes, especially the N−H and C−H stretching region (3250−3400 cm^{-1}), exhibit a prominent red shift in the entire compression region for both α- and δ-$FAPbI_3$ (Tables S3 and S4), indicating pressure-induced enhancement of hydrogen bond interactions. The pressure-induced mode softening of the X−H bond has been widely accepted as strong evidence for the formation and enhancement of the X−H···Y hydrogen bond causing the weakening of the X−H bond.[31] MD simulation reveals that the rotations of FA molecules are reduced at high pressure to ordered oscillations (C as the pivot point), which engages a stronger hydrogen bonding between the FA and PbI_6 via highly effective H···I interactions, with the shortest H···I distance of 2.4 Å (see Figure S7). In contrast to the MA-based counterparts, the FA perovskite is clearly influenced by hydrogen bonding, which, in turn, causes the polymorphic transitions to be significantly different from the former.

Critical to photovoltaics applications, optical response of $FAPbI_3$ was examined as a function of pressure using an optical microscope (Figures 3a and S8) and PL spectroscopy (Figure 3b,c). Upon compression to 4.5 GPa near the amorphization threshold, α-$FAPbI_3$ gradually changes from black to a prominent red and maintains this color at higher pressures.

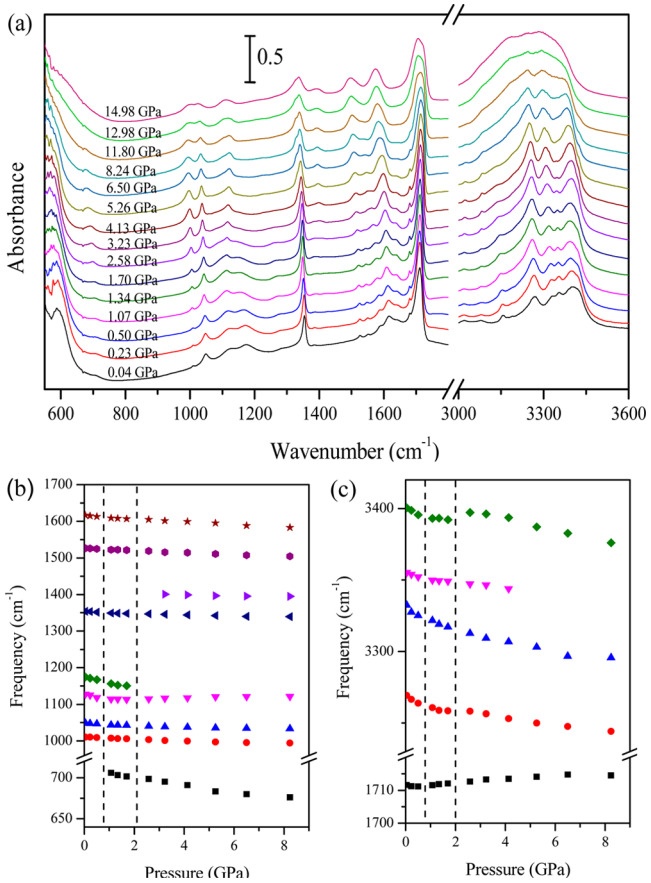

Figure 2. FTIR spectra of α-$FAPbI_3$ upon compression (a) and pressure dependence of selected IR modes (b) and (c).

The color reverses to black after pressure release. In contrast, the δ-phase initially remains yellow but gradually darkens to orange at 6.4 GPa and finally becomes red at higher pressures. Unique piezochromism observed here when compared to other organolead halide perovskite materials[14,15,22] suggests that the optical properties of perovskite materials are structure-dependent and cation-specific. At ambient pressure, a PL peak was observed at 838 nm (1.48 eV) for α-$FAPbI_3$, close to the band gap energy (1.45 eV). Upon compression, the peak shifted to red and exhibited a split profile with an additional PL channel. The pressure-induced additional PL channel was also observed in hybrid organolead halide perovskite materials (e.g., $MAPb(Br_{0.6}I_{0.4})_3$).[14] Therefore, it is highly likely that the non-equivalent iodine ligands in the pressure-distorted PbI_6 octahedra give rise to new PL states. Upon further compression, the major PL channel underwent an abrupt red shift at 1.73 GPa. Above 3.6 GPa, both channels were suppressed. Upon decompression, the PL was recovered with a modified profile and peak position of 824 nm. The evolution of PL peaks shows that the band gap energy reaches a minimum of 1.42 eV at about 3 GPa and then increases. This is in contrast to a recent optical measurement on α-$FAPbI_3$, where the band gap has a monotonic reduction under pressure (to 1.337 eV)[28] in a single structure. Without structural changes, the lattice contraction would play the major role in regulating the PL energy levels. With the lattice distortion and amorphization, however, they outweigh the lattice contraction and lead to the widening of the band gap and total suppression of the PL activity.[22] Moreover, the pressure-induced new PL

DOI: 10.1021/acs.jpclett.7b00665
J. Phys. Chem. Lett. 2017, 8, 2119−2125

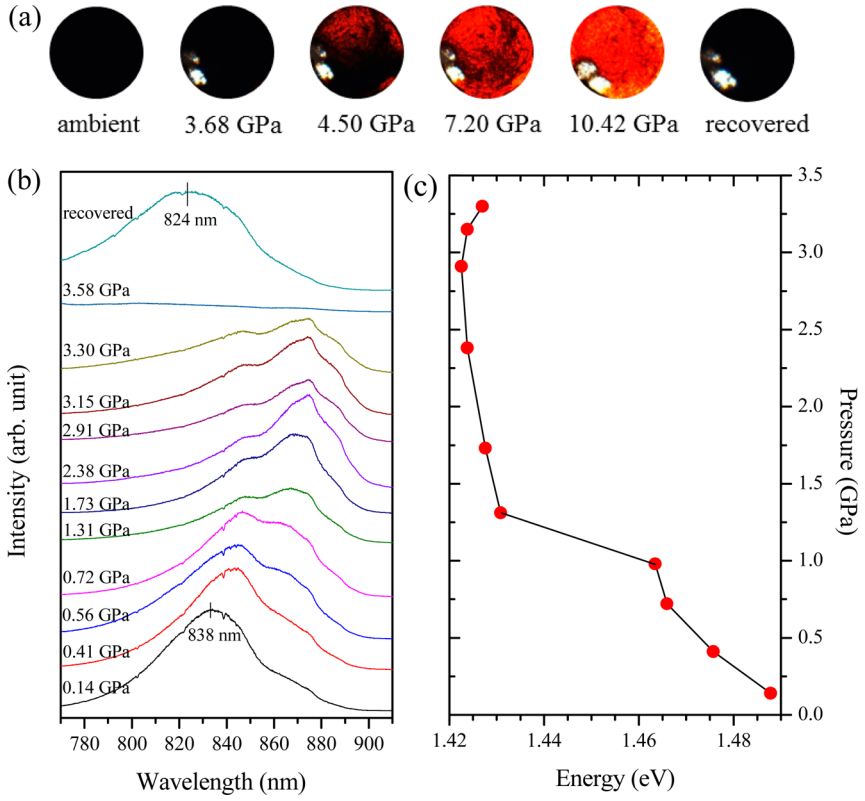

Figure 3. Optical micrographs of α-$FAPbI_3$ upon compression and recovery (a), PL spectra of α-$FAPbI_3$ upon compression and decompression (b), and the corresponding pressure dependence (c).

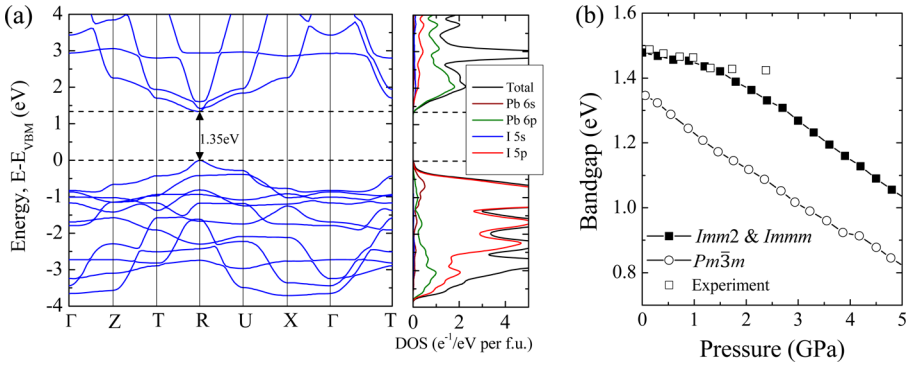

Figure 4. Band structures and projected DOS of α-$FAPbI_3$ (a) at ambient pressure and the calculated band gap energy vs pressure (b).

channels provide a new approach in tuning optical properties in addition to traditional chemical approaches.

The electronic band structure and density of states (DOS) (Figures 4 and S9) reveal that in $FAPbI_3$ the valence bands are dominated by I 5p orbitals. The FA cation has notable contributions to only the conduction bands. The α-$FAPbI_3$ is a direct band gap semiconductor with a calculated band gap energy of 1.35 eV at ambient pressure. The experimental band gap energies are well matched to the *Imm*2 and *Immm* structures. With increasing pressure, the band structures do not have fundamental changes (Figure S9), but the band gap energy decreases (Figure 4b). This agrees with the experiment except the amorphization-induced band gap change near 3 GPa cannot be examined in the crystalline phase. The reduction of the band gap suggests a greater level of orbital overlap in the PbI_6 octahedra, which is naturally induced by the Pb−I bond contraction at high pressure. The FA cations, on the other hand, only have a minor role in determining the band gap. The δ-$FAPbI_3$ has an indirect band gap with E_g = 2.5 eV at ambient pressure, which also reduces with pressure (Figure S10). At high pressure, the δ-phase is distorted to a *C*2/*c* structure, which has a larger band gap compared to the undistorted $P6_3mc$ phase. Here the increase of the band gap is due to distortion within the PbI_6 octahedra, which deviates from the ideal O_h geometry to a distorted square-planar configuration, as a result of molecular tiling and meshing at high pressure. Apparently, the band gaps in both structures can be tuned effectively within a few GPa range. This suggests the possibility of functional manipulation of larger band gap materials to photovoltaic active materials utilizing the externally applied pressure.

Finally, we investigated the EC of both polymorphs, as shown in Figure 5. Near ambient pressure, the α- and δ-$FAPbI_3$ have respective resistances of 1.1×10^9 and 1.7×10^{11} Ohm. The resistance difference is consistent with the relative order of

DOI: 10.1021/acs.jpclett.7b00665
J. Phys. Chem. Lett. 2017, 8, 2119−2125

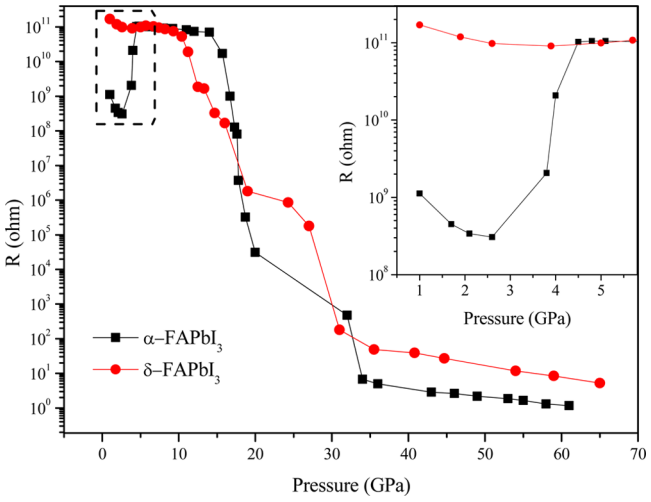

Figure 5. Electrical resistance of the α- and δ-phases of $FAPbI_3$ as a function of pressure. The inset shows a detailed comparison of the electrical resistance of α- and δ-phases of $FAPbI_3$ in the pressure region of 0−5 GPa.

the band gap energies (i.e., 1.45 vs 2.48 eV) and the direct vs indirect band structures as well. However, the absolute values for both polymorphs are surprisingly high for a semiconductor. Here the sample size, thickness, particle packing, grain boundaries, as well as the distortion of the FA cations may physically influence the electrical measurement (see the SI). With increasing pressure, the resistance of α-$FAPbI_3$ reduced significantly to 3.1×10^8 Ohm at 2.6 GPa, but for δ-$FAPbI_3$, the reduction was minor (Figure 5 inset). The dramatic reduction in the former coincides with the structural transitions, while the minor change in the latter is a reflection of structural distortion to a less degree. For both cases, the pressure-induced reduction can be attributed to contraction of the PbI_6 octahedra. Upon compression to 4.5 GPa, the resistance of α-$FAPbI_3$ rapidly increased by 2 orders of magnitude followed by a plateau region until 15 GPa (11 GPa for the δ-phase), where the conductivity was predominated by amorphization.[22] After that, the conductivity dramatically increased by over 9 orders of magnitude as a result of compression to around 35 GPa for both polymorphs, indicating the appearance of a metallic state. To verify this, we performed low-temperature measurements of resistance at different pressures (Figure S11). From the contrasting temperature dependence of resistance of semiconductors and metals, we can propose that the semiconductor-to-metal transitions for α- and δ-$FAPbI_3$ occur at 53 and 41 GPa, respectively. The pressure-induced metallization of $FAPbI_3$ is consistent with theoretical predictions of monotonic decreasing band gap energies.

Overall, the XRD, IR, PL, and electrical measurements collectively revealed contrasting stabilities of two polymorphs of $FAPbI_3$. The optical and electrical properties of α-$FAPbI_3$ are more susceptible to external compression, indicating lower stability compared to δ-$FAPbI_3$, which is consistent with reported relative chemical stabilities. In photovoltaic applications, pressure-tuned new polymorphs from promising precursors offer excellent opportunities to develop performance-improved devices. It would be particularly interesting to evaluate pressure-modified materials (e.g., recovered *Imm*2 structure) in the fabrication of solar cell devices. Moreover, our observations suggest that although the FA cations have limited contribution to the properties they influence the overall structural stability via cation−anion interactions topologically. So far, studies on perovskite materials are primarily focused on the mixed halide moiety in the form of $MAPbI_xBr_{3-x}$. It would be interesting to explore the possibility of mixing cations, such as $MA_xFA_{(1-x)}PbBr_3$ or $MA_xFA_{(1-x)}PbI_3$ for structural studies and photovoltaic applications.

In summary, we investigated structures and properties of $FAPbI_3$ in two polymorphs comparatively by using in situ synchrotron XRD, FTIR spectroscopy, PL spectroscopy, EC measurements, and ab initio simulations. We observed two phase transitions for α-$FAPbI_3$ at 0.3 and 1.7 GPa but only structural distortions for δ-$FAPbI_3$ upon compression. The new structures were identified using XRD with the assistance of MD simulations. The structural modifications in both polymorphs are strongly mediated by the hydrogen bond, as manifested by in situ FTIR spectroscopy unambiguously. The α-$FAPbI_3$ exhibits pressure-dependent PL activities revealing structure-regulated band gaps, which was excellently reproduced by DFT calculations. Finally, α- and δ-$FAPbI_3$ exhibit strongly contrasting pressure-regulated dc conductivities in the low-pressure region, but both approach metallic states at high pressures. These observations suggest that external compression can not only reveal contrasting structural stabilities but effectively tune the optoelectric properties of both polymorphs. Our study thus provides valuable insight into the design and engineering of organolead halide perovskite-based solar cell materials.

EXPERIMENTAL SECTION

We synthesized both α- and δ-phase $FAPbI_3$ using the previously reported methods.[2,29] The synthesized samples were characterized by XRD using Co Kα radiation to check the phase identity and purity. Static high pressure was achieved using diamond anvil cells with various culet sizes and different optical types. In situ angle dispersive high-pressure X-ray microdiffraction measurements were carried out at Sector 20 ID of the Advanced Photon Source, Argonne National Laboratory. The in situ high-pressure FTIR spectroscopy was conducted using a customized FTIR microscope. The optical microphotographs were collected from a Leica stereomicroscope. PL measurements were carried out using a customized Raman spectrometer with a 532 nm excitation laser. The in situ EC measurements were done using the Maglab system. All calculations were performed using the projector-augmented planewave (PAW) method[32] with first-principles implementations of DFT in the Vienna Ab Initio Simulation (VASP) program.[33] See the Supporting Information for experimental and computational details.

ASSOCIATED CONTENT

Supporting Information

The Supporting Information is available free of charge on the ACS Publications website at DOI: 10.1021/acs.jpclett.7b00665.

Additional experimental and computational details, XRD analysis of δ-$FAPbI_3$, structural information, IR spectroscopic analysis, band structure calculations, and electrical conductivity at low temperatures (PDF)

AUTHOR INFORMATION

Corresponding Author

*E-mail: yang.song@uwo.ca.

DOI: 10.1021/acs.jpclett.7b00665
J. Phys. Chem. Lett. 2017, 8, 2119−2125

ORCID

Yang Song: 0000-0001-7853-3737

Notes

The authors declare no competing financial interest.

■ ACKNOWLEDGMENTS

This work was supported by two Discovery Grants, a RTI Grant from NSERC of Canada, a Leaders Opportunity Fund from the Canadian Foundation for Innovation, and an Early Researcher Award from the Ontario Ministry of Research and Innovation. We thank Dr. C. Sun for his technical assistance in the XRD experiments. This work was partially performed at Sector 20, Advanced Photon Source (APS), Argonne National Laboratory, supported by the U.S. Department of Energy and the Canadian Light Source. Computing resources were provided by the University of Saskatchewan, WestGrid, and Compute Canada.

■ REFERENCES

(1) Service, R. F. Perovskite Solar Cells Keep On Surging. *Science* **2014**, *344*, 458−458.

(2) Jeon, N. J.; Noh, J. H.; Yang, W. S.; Kim, Y. C.; Ryu, S.; Seo, J.; Seok, S. I. Compositional Engineering of Perovskite Materials for High-Performance Solar Cells. *Nature* **2015**, *517*, 476−480.

(3) Eperon, G. E.; Stranks, S. D.; Menelaou, C.; Johnston, M. B.; Herz, L. M.; Snaith, H. J. Formamidinium Lead Trihalide: A Broadly Tunable Perovskite for Efficient Planar Heterojunction Solar Cells. *Energy Environ. Sci.* **2014**, *7*, 982−988.

(4) Saliba, M.; Matsui, T.; Seo, J. Y.; Domanski, K.; Correa-Baena, J. P.; Nazeeruddin, M. K.; Zakeeruddin, S. M.; Tress, W.; Abate, A.; Hagfeldt, A.; et al. Cesium-Containing Triple Cation Perovskite Solar Cells: Improved Stability, Reproducibility and High Efficiency. *Energy Environ. Sci.* **2016**, *9*, 1989−1997.

(5) Zhou, H. P.; Chen, Q.; Li, G.; Luo, S.; Song, T. B.; Duan, H. S.; Hong, Z. R.; You, J. B.; Liu, Y. S.; Yang, Y. Interface Engineering of Highly Efficient Perovskite Solar Cells. *Science* **2014**, *345*, 542−546.

(6) Noh, J. H.; Im, S. H.; Heo, J. H.; Mandal, T. N.; Seok, S. I. Chemical Management for Colorful, Efficient, and Stable Inorganic-Organic Hybrid Nanostructured Solar Cells. *Nano Lett.* **2013**, *13*, 1764−1769.

(7) Pang, S. P.; Hu, H.; Zhang, J. L.; Lv, S. L.; Yu, Y. M.; Wei, F.; Qin, T. S.; Xu, H. X.; Liu, Z. H.; Cui, G. L. $NH_2CH{=}NH_2PbI_3$: An Alternative Organolead Iodide Perovskite Sensitizer for Mesoscopic Solar Cells. *Chem. Mater.* **2014**, *26*, 1485−1491.

(8) Grochala, W.; Hoffmann, R.; Feng, J.; Ashcroft, N. W. The Chemical Imagination at Work in Very Tight Places. *Angew. Chem., Int. Ed.* **2007**, *46*, 3620−3642.

(9) Yang, W. S.; Noh, J. H.; Jeon, N. J.; Kim, Y. C.; Ryu, S.; Seo, J.; Seok, S. I. High-Performance Photovoltaic Perovskite Layers Fabricated Through Intramolecular Exchange. *Science* **2015**, *348*, 1234−1237.

(10) Capitani, F.; Marini, C.; Caramazza, S.; Postorino, P.; Garbarino, G.; Hanfland, M.; Pisanu, A.; Quadrelli, P.; Malavasi, L. High-Pressure Behavior of Methylammonium Lead Iodide ($MAPbI_3$) Hybrid Perovskite. *J. Appl. Phys.* **2016**, *119*, 185901.

(11) Stoumpos, C. C.; Malliakas, C. D.; Kanatzidis, M. G. Semiconducting Tin and Lead Iodide Perovskites with Organic Cations: Phase Transitions, High Mobilities, and Near-Infrared Photoluminescent Properties. *Inorg. Chem.* **2013**, *52*, 9019−9038.

(12) Wang, Z. W.; Zhou, Y. Y.; Pang, S. P.; Xiao, Z. W.; Zhang, J. L.; Chai, W. Q.; Xu, H. X.; Liu, Z. H.; Padture, N. P.; Cui, G. L. Additive-Modulated Evolution of $HC(NH_2)_2PbI_3$ Black Polymorph for Mesoscopic Perovskite Solar Cells. *Chem. Mater.* **2015**, *27*, 7149−7155.

(13) Weller, M. T.; Weber, O. J.; Frost, J. M.; Walsh, A. Cubic Perovskite Structure of Black Formamidinium Lead Iodide, α-$[HC(NH_2)_2]PbI_3$, at 298 K. *J. Phys. Chem. Lett.* **2015**, *6*, 3209−3212.

(14) Jaffe, A.; Lin, Y.; Beavers, C. M.; Voss, J.; Mao, W. L.; Karunadasa, H. I. High-Pressure Single-Crystal Structures of 3D Lead-Halide Hybrid Perovskites and Pressure Effects on their Electronic and Optical Properties. *ACS Cent. Sci.* **2016**, *2*, 201−209.

(15) Wang, L. R.; Wang, K.; Zou, B. Pressure-Induced Structural and Optical Properties of Organometal Halide Perovskite-Based Formamidinium Lead Bromide. *J. Phys. Chem. Lett.* **2016**, *7*, 2556−2562.

(16) Jiang, S. J.; Fang, Y. A.; Li, R. P.; Xiao, H.; Crowley, J.; Wang, C. Y.; White, T. J.; Goddard, W. A.; Wang, Z. W.; Baikie, T.; et al. Pressure-Dependent Polymorphism and Band-Gap Tuning of Methylammonium Lead Iodide Perovskite. *Angew. Chem., Int. Ed.* **2016**, *55*, 6540−6544.

(17) Ou, T. J.; Yan, J. J.; Xiao, C. H.; Shen, W. S.; Liu, C. L.; Liu, X. Z.; Han, Y. H.; Ma, Y. Z.; Gao, C. X. Visible Light Response, Electrical Transport, and Amorphization in Compressed Organolead Iodine Perovskites. *Nanoscale* **2016**, *8*, 11426−11431.

(18) Szafranski, M.; Katrusiak, A. Mechanism of Pressure-Induced Phase Transitions, Amorphization, and Absorption-Edge Shift in Photovoltaic Methylammonium Lead Iodide. *J. Phys. Chem. Lett.* **2016**, *7*, 3458−3466.

(19) Wang, K.; Liu, R.; Qiao, Y.; Cui, J.; Song, B.; Liu, B.; Zou, B. Pressure-Induced Reversible Phase Transition and Amorphization of $CH_3NH_3PbI_3$. *Acta. Phys. Sin* **2017**, *66*, 030701.

(20) Lee, Y.; Mitzi, D. B.; Barnes, P. W.; Vogt, T. Pressure-Induced Phase Transitions and Templating Effect in Three-Dimensional Organic-Inorganic Hybrid Perovskites. *Phys. Rev. B: Condens. Matter Mater. Phys.* **2003**, *68*, 020103.

(21) Swainson, I. P.; Tucker, M. G.; Wilson, D. J.; Winkler, B.; Milman, V. Pressure Response of An Organic-Inorganic Perovskite: Methylammonium Lead Bromide. *Chem. Mater.* **2007**, *19*, 2401−2405.

(22) Wang, Y. H.; Lu, X. J.; Yang, W. G.; Wen, T.; Yang, L. X.; Ren, X. T.; Wang, L.; Lin, Z. S.; Zhao, Y. S. Pressure-Induced Phase Transformation, Reversible Amorphization, and Anomalous Visible Light Response in Organolead Bromide Perovskite. *J. Am. Chem. Soc.* **2015**, *137*, 11144−11149.

(23) Lü, X.; Wang, Y.; Stoumpos, C. C.; Hu, Q.; Guo, X.; Chen, H.; Yang, L.; Smith, J. S.; Yang, W.; Zhao, Y.; et al. Enhanced Structural Stability and Photo Responsiveness of $CH_3NH_3SnI_3$ Perovskite via Pressure-Induced Amorphization and Recrystallization. *Adv. Mater.* **2016**, *28*, 8663−8668.

(24) Matsuishi, K.; Ishihara, T.; Onari, S.; Chang, Y.; Park, C. Optical Properties and Structural Phase Transitions of Lead-Halide Based Inorganic-Organic 3D and 2D Perovskite Semiconductors Under High Pressure. *Phys. Status Solidi B* **2004**, *241*, 3328−3333.

(25) Li, Q.; Li, S. R.; Wang, K.; Quan, Z. W.; Meng, Y.; Zou, B. High-Pressure Study of Perovskite-Like Organometal Halide: Band-Gap Narrowing and Structural Evolution of $[NH_3\text{-}(CH_2)_4\text{-}NH_3]CuCl_4$. *J. Phys. Chem. Lett.* **2017**, *8*, 500−506.

(26) Wang, L. R.; Wang, K.; Xiao, G. J.; Zeng, Q. S.; Zou, B. Pressure-Induced Structural Evolution and Band Gap Shifts of Organometal Halide Perovskite-Based Methylammonium Lead Chloride. *J. Phys. Chem. Lett.* **2016**, *7*, 5273−5279.

(27) Jaffe, A.; Lin, Y.; Mao, W. L.; Karunadasa, H. I. Pressure-Induced Conductivity and Yellow-to-Black Piezochromism in a Layered Cu-Cl Hybrid Perovskite. *J. Am. Chem. Soc.* **2015**, *137*, 1673−1678.

(28) Liu, G.; Kong, L. P.; Gong, J.; Yang, W. G.; Mao, H. K.; Hu, Q. Y.; Liu, Z. X.; Schaller, R. D.; Zhang, D. Z.; Xu, T. Pressure-Induced Bandgap Optimization in Lead-Based Perovskites with Prolonged Carrier Lifetime and Ambient Retainability. *Adv. Funct. Mater.* **2017**, *27*, 1604208.

(29) Wozny, S.; Yang, M. J.; Nardes, A. M.; Mercado, C. C.; Ferrere, S.; Reese, M. O.; Zhou, W. L.; Zhu, K. Controlled Humidity Study on the Formation of Higher Efficiency Formamidinium Lead Triiodide-Based Solar Cells. *Chem. Mater.* **2015**, *27*, 4814−4820.

(30) Koh, T. M.; Fu, K. W.; Fang, Y. N.; Chen, S.; Sum, T. C.; Mathews, N.; Mhaisalkar, S. G.; Boix, P. P.; Baikie, T. Formamidinium-Containing Metal-Halide: An Alternative Material for Near-IR

DOI: 10.1021/acs.jpclett.7b00665
J. Phys. Chem. Lett. 2017, 8, 2119−2125

Absorption Perovskite Solar Cells. *J. Phys. Chem. C* **2014**, *118*, 16458−16462.
(31) Zhou, L.; Shinde, N.; Hu, A. G.; Cook, C.; Murugesu, M.; Song, Y. Structural Tuning of Energetic Material Bis(1H-tetrazol-5-yl)amine Monohydrate under Pressures Probed by Vibrational Spectroscopy and X-ray Diffraction. *J. Phys. Chem. C* **2014**, *118*, 26504−26512.
(32) Kresse, G.; Joubert, D. From Ultrasoft Pseudopotentials to the Projector Augmented-Wave Method. *Phys. Rev. B: Condens. Matter Mater. Phys.* **1999**, *59*, 1758−1775.
(33) Kresse, G.; Hafner, J. Abinitio Molecular-Dynamics for Liquid-Metals. *Phys. Rev. B: Condens. Matter Mater. Phys.* **1993**, *47*, 558−561.

DOI: 10.1021/acs.jpclett.7b00665
J. Phys. Chem. Lett. 2017, 8, 2119−2125